Recovery of zinc from scrap steel using zinc–bromine battery technology

Authors: Mr. Rhys Standing [a], Dr. Christian J. Laycock [a] *, Dr. Gareth Lloyd [b], Prof. Richard M. Dinsdale [a] and Prof. Alan J. Guwy [a]

[a] Sustainable Environment Research Centre, University of South Wales, Upper Glyntaff, Pontypridd, CF37 4BD, United Kingdom

[b] Tata Steel Strip Products, Neath Port Talbot, Port Talbot, SA13 2NG, United Kingdom

* Corresponding author.

Email: christian.laycock@southwales.ac.uk

Tel: +44 (0)1443 654596

Abstract

Secondary production of steel is proven to significantly decrease CO_2 emissions of steelmaking, but only 40 % of steel is produced via recycling, which is made difficult by contamination of scrap resources with non-ferrous metals and non-metal debris. These contaminants include zinc, which blast furnace and electric arc systems have a low tolerance towards (< 0.02 wt%). In this work, clean and efficient recovery of zinc from the surface of steel substrates was investigated using a custom-made low-cost membrane-free non-flow zinc-bromine battery (ZBB) that enabled rapid and straightforward integration and removal of steel substrates. The electrical performance of the cell was characterised by charge-discharge profiles, and zinc removal and recovery onto electrodes was characterised using Scanning Electron Microscopy (SEM) and Energy Dispersive Spectroscopy (EDS). Upon discharging, the cell efficiently removed > 99.9 wt% zinc from steel surfaces. On recharging the cell, zinc was re-electroplated onto a carbon foam electrode in an easily recoverable form and with high purity. The process was repeated over 30 cycles to demonstrate robustness. The work shows the importance of the cut-off voltage upon discharging: if less than 0.5 V, the cell co-extracted iron into the electrolyte solution, affecting cell durability and zinc purity. A two-stage process for recovering zinc from scrap steel is proposed, illustrating how ZBB technology could enable efficient and clean recovery of zinc from complex scrap steel resources in the steel industry.

Keywords

Scrap steel, steel recycling, non-flow battery, static battery, membrane-free battery.

Introduction

Stainless steel is an extremely important and versatile material with applications across many sectors including construction, manufacturing, healthcare, food and chemicals.[1] It is utilised ubiquitously throughout society, with steel manufacturing widely used as an indicator of economic growth.[2] However, primary manufacturing of steel from virgin iron ore and coal is a highly energy intensive process requiring a cumulative energy input of 15-24 GJ t^{-1}.[3] The iron and steel industry is a significant contributor to global warming and accounts for between 4-7 % of global anthropogenic CO_2 emissions. In addition to greenhouse gas emissions, primary steel manufacturing processes also yield a range of complex waste streams and by-products that contribute to well-established public health and environmental problems. In order for the steel industry to reach net zero targets and be less polluting, significant technical innovations will be required to enable manufacturing of green steel as well as effective and efficient processes for recycling and re-using scrap, waste and by-product streams.

Secondary steel production (recycling) involves re-melting of scrap steel and presents an opportunity to significantly reduce CO_2 emissions, since it requires less energy with a cumulative energy consumption of 1.3-6.0 GJ t^{-1}.[2] At present, only 40 % of steel is produced via secondary methods and therefore increasing steel recycling rates offers significant scope to decrease CO_2 emissions.[3] The challenges faced by recycling end-of-life scrap steel mainly relate to contamination with non-steel metals and non-metal debris, which arises due to imperfect (or non-existent) separation processes.[4] If present, impurities may produce a melt with an unsuitable composition and they must either be removed by improved separation, or (more commonly) the scrap is diluted with primary pig iron until impurities fall within acceptable levels. The latter ensures recycling but in effect decreases the rate of secondary steel production. Increasing the utilisation of end-of-life scrap steel whilst avoiding dependence on primary pig iron will require effective, efficient and clean separation of materials and alloys to be developed and deployed.[3]

Many types of steel are galvanised by coating with a thin layer of zinc via hot-dip coating processes. Zinc provides a protective barrier towards corrosive elements and, amongst other things, prevents

rusting.[5,6] Upon re-melting galvanised steel in a blast furnace, zinc-containing materials are firstly reduced to metallic zinc, which has a relatively low boiling point (907 °C) compared with blast furnace operating temperatures (1600-1650 °C). The zinc evaporates and then condenses upon cooling, with some zinc depositing on the walls of the furnace and the rest forming a component of dust effluents collected during flue gas cleaning processes.[7] In order to prevent technical difficulties caused by zinc deposits, the zinc content of the melt is typically limited to 0.012-0.020 wt% for most blast furnace operations.[8,9] The concentration of zinc in the dust effluent is around 2-30 wt% for electric arc furnaces and 0.4-2.8 wt% for blast furnaces, which is too high for remelting. In the case of blast furnaces, the concentration of zinc is too low for economical recovery, whilst levels of electrical arc furnace dust are more favourable.[10] Despite these challenges, recovery of zinc from steel has wider importance, since it is estimated that without improvements to the recovery rate of secondary zinc, proven reserves will be exhausted as early as 2050.[11]

Presently deployed methods for recovering zinc from dust waste include the Waelz process, which is a pyrometallurgical process involving heat treatment of zinc wastes using a carbon-based fuel at temperatures in excess of 1,000 °C in a rotating kiln. The zinc compounds are reduced, evaporated and re-oxidised in the gas phase, separating zinc from ferrous materials.[7] These methods are very efficient (with zinc removal rates of approx. 90 %),[12] but are also energy intensive and yield hazardous residues which are problematic to dispose of. In addition, the Waelz process is not economically viable when the zinc loading is below 10 wt%. Other zinc recovery methods include hydrometallurgical processes such as alkaline leaching, which are typically used for recovering zinc from the dust effluents produced by electric arc furnaces.[13] Like pyrometallurgical processes, these processes are best suited to high zinc loadings and also yield problematic by-product streams.[14] In general, pyrometallurgical and hydrometallurgical zinc recovery processes are more applicable to electrical arc furnace dusts and neither are capable of economic extraction of zinc from blast furnace dust.[7,15]

In this work, the recovery of zinc from end-of-life scrap was investigated by using a membrane-free non-flow zinc-bromine battery (ZBB) to recover zinc from steel substrates. Recovery of zinc directly from steel was investigated because upstream removal avoids subsequent damage to blast furnaces and

the need to recover zinc from dusts, either by diluting in pig iron or through complex extraction processes. This paper includes a brief literature review of ZBB technology, which was chosen because the fundamental chemistry of these devices theoretically enables the recovery of zinc from metal structures and substrates without production of harmful or problematic by-products. A non-flow battery design with an aqueous liquid electrolyte was chosen due to the low-cost materials and low balance-of-plant costs this gives. The architecture and design of the battery were customised in order to produce a robust system that potentially enables fast and automated dipping of steel substrates and waste streams without modifications to or disassembly of the cell. The electrochemical performance of the cell was characterised by measurement of charge-discharge profiles and the removal and recovery of zinc was characterised by scanning electron microscopy and energy dispersive spectroscopy.

Redox flow zinc-bromine batteries

A zinc-bromine battery (ZBB) is a rechargeable electrochemical cell that operates according to reactions (1-3). Zinc-bromine batteries have been more widely studied and developed with a redox flow battery design, in which high surface area carbon plastic electrodes are placed inside two electrolyte compartments separated by an ion-conducting membrane typically made with a microporous polyolefin (see Fig. 1).[16] Cells have an electrolyte solution composed of aqueous zinc bromide ($ZnBr_2$) which is pumped continuously through the electrolyte compartments from external storage tanks. When charging, aqueous zinc ions are conducted through the membrane to the anode/anolyte side of the cell and converted into metallic zinc according to reaction (1). The metallic zinc is heterogeneously deposited from the liquid to the solid phase onto a carbon-based electrode. At the cathode/catholyte side of the cell, aqueous bromine ions are converted into bromine liquid as described by reaction (2),[17] to complete the overall reaction (3).

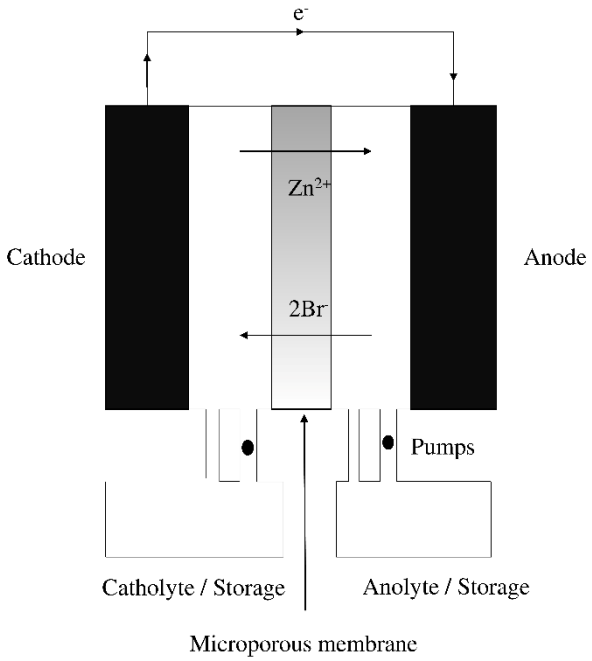

Figure 1. Schematic showing the operation of a zinc-bromine redox flow battery.

$$Zn^{2+}_{(aq)} + 2e^- \leftrightarrow Zn_{(s)} \ (E^o = -0.76 \text{ V}) \quad (1)$$

$$2Br^-_{(aq)} \leftrightarrow Br_{2\,(l)} + 2e^- \ (E^o = 1.08 \text{ V}) \quad (2)$$

$$\text{Overall reaction: } Zn^{2+}_{(aq)} + 2Br^-_{(aq)} \leftrightarrow Br_{2\,(l)} + Zn_{(s)} \ (E^o = 1.84 \text{ V}) \quad (3)$$

A bromine complexing agent (such as *N*-ethyl-*N*-methyl-pyrrolidinium bromide) is also present on the catholyte side for the purposes of bromine storage; the complexing agent forms a heavy oil which sinks to the bottom of the external storage tank. Once fully charged, an open circuit voltage of approx. 1.84 V is achieved. When discharging, all processes take place in reverse, yielding electrical power and restoring the electrolyte solutions to aqueous zinc bromide.

Zinc-bromine flow batteries have attracted increasing interest in recent decades due to their high voltage, high energy density and high current density compared with other redox flow batteries (such as vanadium-based and lead-acid flow batteries), making them potentially very attractive systems for stationary energy storage applications.[18-21] They are scalable, require low-cost, non-hazardous and clean materials, and are made with well-understood and easily serviceable components such as pumps. As such, they are potentially very robust systems that can achieve a cost-effective and long operational

life.[17.22] Challenges of zinc-bromine flow battery deployment relate to their low specific power, energy density and electrical efficiencies compared with lithium-ion batteries. There is also the risk of self-discharge, which may occur due to excessive accumulation of bromine or zinc at the electrodes. Furthermore, whilst ancillary components such as pumps are widely available and well understood, they drastically increase the overall cost of a cell,[23,24] meaning the balance-of-plant costs outweigh the low costs of the active materials. These factors mean that the cost of power from ZBB technology is much higher compared with state-of-the-art battery technology, and the high system capital costs are a significant barrier to the commercialisation and deployment of redox flow ZBB technology.[18,23-25]

A comprehensive review of ZBBs was conducted by Xu *et al*.[26] in which electrode materials, cell design, electrolytes and membranes were described comprehensively. Carbon-based materials are the most widely used type of electrode because they have a large surface area, high electrical conductivity, high catalytic activity towards the electrochemical reactions as well as good chemical stability. They are also widely available, relatively low cost and can be made in various forms and shapes (carbon felt, vitreous carbon and carbon foam). Alternatively, metallic electrodes can be used such as titanium. Metallic electrodes typically have faster kinetics, lower charge transfer resistance and higher electrical conductivity than carbon-based materials and generally result in superior overall cell performance.[27,28] However, they are more expensive and prone to degradation mechanisms such as corrosion, affecting the long-term durability of the cell.[29]

The primary electrochemically active electrolyte component in ZBB flow batteries is aqueous zinc bromide, which is usually present in concentrations ranging between 1-4 M.[30] In addition to zinc bromide, the electrolyte solution often contains supporting electrolyte salts in order to enhance ionic conductivity and reduce internal resistance.[31] Commonly used salts such as sodium chloride and potassium chloride (2 M) are suitable due to their lack of interference with bromine reduction.[32] However, over long time periods, chlorides can negatively impact cell performance due to the susceptibility of zinc to corrosion from chloride-based species.[33]

The membrane is a key component of the cell which physically separates the anolyte and catholyte solutions whilst allowing selective transfer of zinc and bromine ions. It is the most expensive single component of ZBB cell, accounting for approximately 22-40% of the cost.[18] Microporous membranes (for example, SF-600 and Daramic®) and ion-exchange membranes (such as Nafion) are the most widely used.[34,35] Microporous membranes typically have a thickness of several hundred microns in order to ensure bromine separation; this is thicker than ion-exchange membranes and therefore they have greater internal resistances.[36] However, if not complexed or stored correctly, high concentrations of bromine may accumulate and more easily diffuse through microporous membranes. In addition, operation over long time periods can lead to the growth of zinc dendrites on the anode, which have a high mechanical strength and can puncture microporous membranes.[37] Nafion membranes give up to 15 % higher coulombic efficiencies than microporous membranes and have a dense structure which increases their mechanical strength and therefore their resilience towards zinc dendrites and ability to physically separate electrolyte liquids.[17] However, Nafion membranes yield a lower voltage efficiency by 12 % due to higher ohmic resistances. Zinc dendrite growth can be alleviated by fully discharging the cell periodically to bring excessive zinc growth back into the aqueous electrolyte phase.[38]

Zinc-bromine flow batteries require a bromine complexing agent in order to prevent bromine gas formation under charging.[39] BCAs decrease the reaction kinetics but overall have a positive impact on cell performance for zinc electro-deposition and zinc electro-dissolution, resulting in higher redox reaction reversibility and activity. Typically, a quaternary ammonium bromide salt is used such as N-Methyl-N-Ethyl Pyrrolidinium Bromide.[40-42] When in solution, these substances form a complex with bromine as a polybromide phase, which has low electrochemical activity and is a higher density oil which sinks to the bottom of the external catholyte storage tank,[43] thereby managing the bromine. In addition to increasing the costs of the cell, complexing agents also decrease the rate of bromine reduction, causing increased voltage losses.[44]

Non-flow zinc-bromine batteries

Non-flow (static) ZBBs are less well-studied than redox flow ZBBs but have key advantages due to their simpler design, which removes the need for ancillary components so that there are no moving parts or pumps, and the balance-of-plant costs are reduced. There is no forced convection and zinc dendrites are allowed to form freely. They also have slightly higher energy densities compared with flow batteries, being capable of operating at 142 Wh kg^{-1} compared with 135 Wh kg^{-1} for flow systems.[45,46] They have higher coulombic efficiencies of up to 99.9 % and energy efficiencies of up to 94.0 %,[45] compared with coulombic efficiencies of 95.0 % and energy efficiencies of 75 % for flow batteries.[46] Within non-flow systems there are liquid- and gel-based batteries, where gel batteries still utilise a membrane but remove other ancillary components. Whilst this does reduce the overall cost, the membrane is still the most expensive component of ZBBs.

A non-flow membrane-free ZBB was initially developed and studied by Biswas *et al*.[46] This cell was composed of a single electrolyte chamber containing an aqueous zinc bromide electrolyte solution, a carbon cloth zinc electrode and a hydrophobic carbon foam bromine electrode, composed of graphite and carbon black (see Fig 2). Under charging, aqueous zinc ions were reduced to form metallic zinc which plated onto the carbon cloth anode. Bromine ions were oxidised to form bromine liquid, which displaced the electrolyte within the pores of the carbon foam electrode. With continued charging, excess bromine liquid spilled out from the pores of the electrode and accumulated within the bottom of the cell due to the higher density of bromine liquid (3.1 g mL^{-1}) compared with the electrolyte solution (1.5 g mL^{-1}). Separation of the bromine and zinc was thus achieved by a physical method in which the zinc electrode was positioned at the top of the cell and the bromine remained at the bottom of the cell due to it's higher density and low miscibility with water. Under charging, zinc dendrites formed and grew downwards towards the bromine liquid and carbon foam electrode. Upon reaching the carbon foam surface, the metallic zinc reacted with the bromine liquid to regenerate aqueous dissolved zinc and bromine ions, thereby preventing short-circuiting of the cell since this process had a faster rate than zinc deposition for charging currents of less than 50 mA. This spontaneous mechanism was key to the operation of the cell because it enabled protection from cell shorting (a well-established challenge of

redox flow ZBBs) without the need for an expensive membrane. Some zinc corrosion was observed to take place due to reaction with Br^{3-} and higher bromine complexes, but this did not contribute significantly to cell operation. This design removed the requirement to pump solutions around the cell, potentially minimising the balance-of-plant costs by removing auxiliary components found in redox flow ZBBs. In addition, this mechanism ensured there would be no irreversible damage to the cell in the event of self-discharge due to zinc corrosion. Under charging, some hydrogen was also generated at the zinc electrode due to the acidic conditions within the cell. However, when using low currents, the amount of hydrogen produced was not significant (< 0.03 % of cell capacity per cycle). It is possible this could be controlled by adapting the cell design and composition to promote hydrogen recapture by reaction with bromine liquid to form hydrobromic acid. In the present design however, this limited the battery to currents of 20 mA cm^{-2} and energy densities of 50 Wh L^{-1}. Discharging the cell was shown to reverse the processes described above, returning the cell to its original state and appearance.[19,45,46]

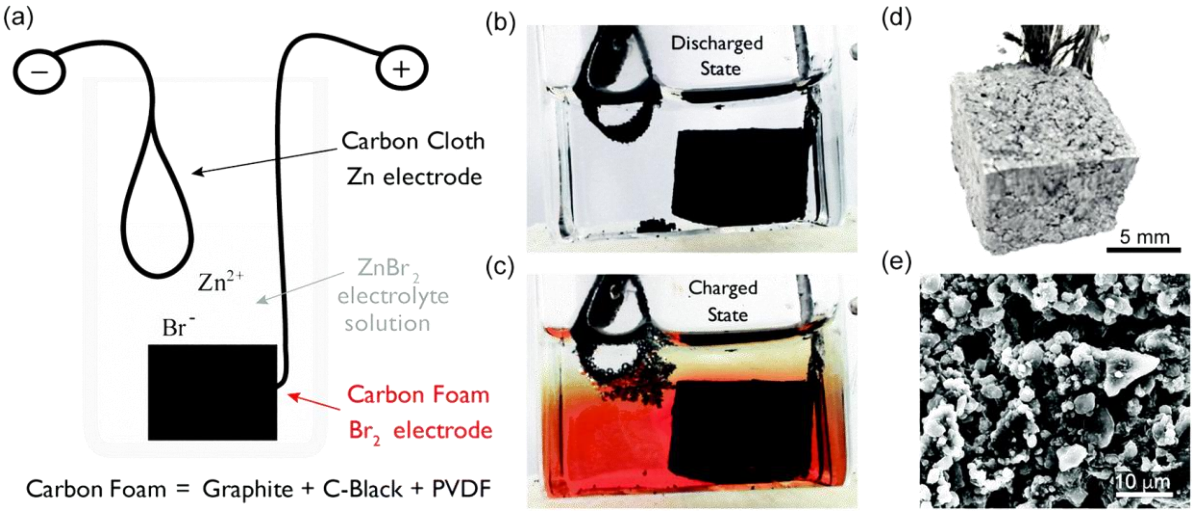

Figure 2. Setup and components of non-flow zinc-bromine battery cell. (taken from [46])

In this work, we have developed and studied a membrane-free non-flow zinc-bromine battery for the purposes of recovering zinc from steel surfaces. The cell was based on the design shown above due to the ease of assembly and simplicity of design which potentially enables clean and efficient recovery of zinc from scrap and waste resources. The design enabled dipping of steel substrates directly into the electrolyte solution without disassembly of the battery housing. In addition, the design involves the use of low-cost materials and reagents and offers low balance-of-plant costs.

Results and Discussion

Steel anode discharge characterisation

Fig. 3 shows photographs of the assembled experimental ZBB cell before and after charging. Before charging (see Fig. 3a), the electrolyte was clear and the carbon foam electrodes were seen clearly, with the bromine electrode (cathode) located at the bottom of the cell and the zinc electrode (anode) dipped into the electrolyte at the top of the cell and held in place using crocodile clips. The cell charged according to the mechanism described by Biswas *et al*.[46] (see Fig. 3b). The electrolyte solution was initially clear and developed a deep orange colour towards the bottom of the cell that was characteristic of concentrated liquid bromine produced due to electrolytic oxidation of bromine ions (see reaction 3). The bromine formed towards the bottom of the electrolyte chamber since it was denser than the electrolyte solution and was accommodated within the pore structure of the carbon foam cathode. The electrolyte solution retained a clear appearance at the top of the cell. Zinc was plated onto the anode and throughout charging, metallic zinc dendrites crystals had grown downwards towards the bromine liquid phase (reaction 3). Upon reaching this interface, the dendrites did not grow further, indicating the presence of zinc corrosion by reaction with bromine liquid to regenerate dissolved aqueous zinc and bromine ions. This enabled the cell to maintain a stable OCV of 1.82 V. Discharging the cell was found to almost fully reverse these observations, returning the cell very closely to the original appearance in Fig. 3a.

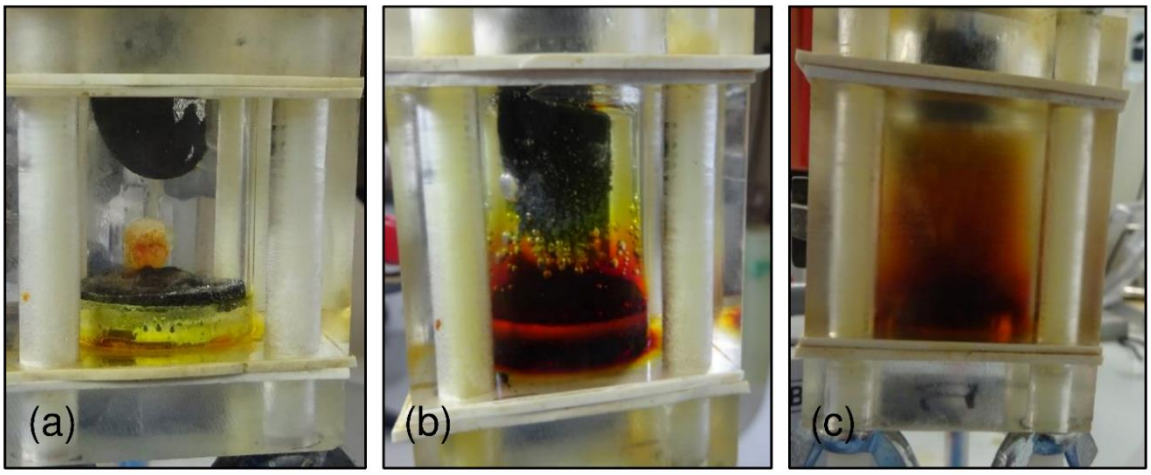

Figure 3. Photographs showing the assembled ZBB experimental cell: (a) before charging, and (b) after charging. (c) shows the cell after discharging with a steel zinc electrode.

The cell was subsequently recharged, and the carbon foam anode was replaced with a 25 × 25 × 2.5 mm piece of galvanised steel. Upon inserting the steel into the cell, the OCV decreased from 1.82 V to 1.70 V. The decrease of OCV is suggested to be due to the presence of non-zinc metals such as iron in the steel. When the cell was discharged, the electrolyte developed an opaque brown/orange colour rather than returning to a transparent appearance. This suggests that in addition to metallic zinc, discharging with steel also extracted some iron into the electrolyte and that discharging was not 100 % selective towards zinc.

Fig. 4 shows discharge profiles measured for separate ZBB cells, with one cell discharged using a carbon foam anode, and the second cell discharged using a galvanised steel anode. Both cells were charged under identical conditions and discharged using a cut-off voltage of 0.2 V. For the carbon anode, there was an initial conditioning period for approx. 5 minutes where the cell potential decreased non-linearly. Following this transient, the cell potential decreased linearly until approx. 25-30 minutes when the cell potential again decreased non-linearly, falling sharply and reaching the cut-off voltage rapidly to complete cell discharge. In conducting this work, the coulombic efficiency was typically measured in the range 55-60 %.

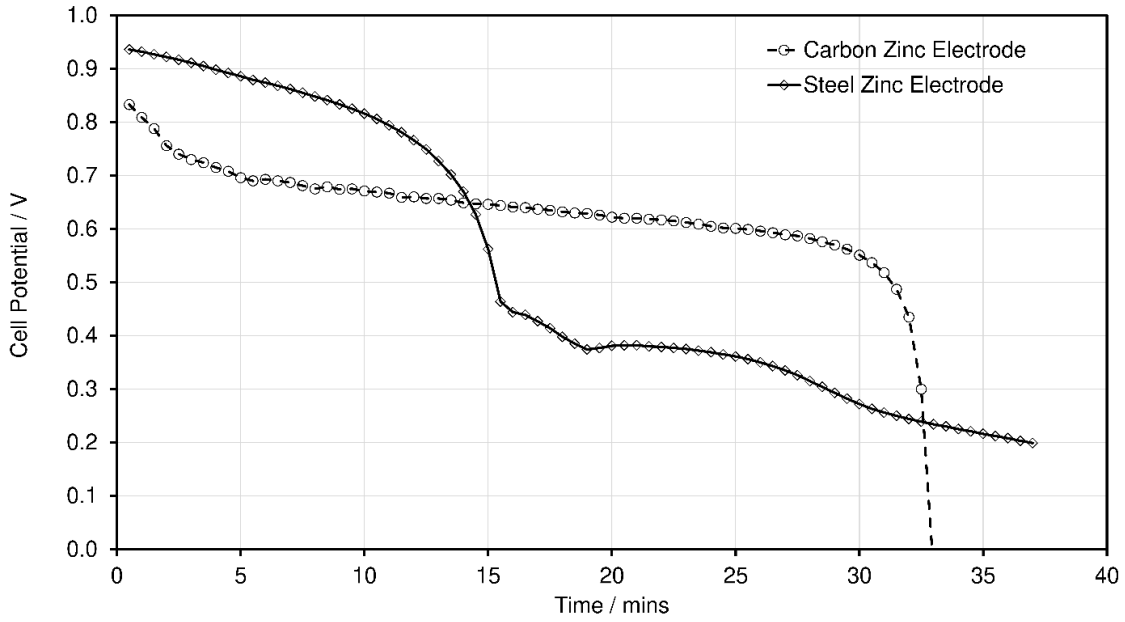

Figure 4. Discharge profiles of separate ZBB cells, where one cell was discharged using a conventional carbon foam anode and the second cell discharged using a galvanised steel anode. Discharge was measured after identical charging regimes. The profiles were measured galvanostatically by applying ± 100 mA of current load to the cell and using cut-off voltages of 2.2 V under charging and 0.2 V under discharging.

The discharge profile measured for the steel anode was markedly different, with a two-stage discharge process observed. Unlike the carbon foam anode, the discharge profile proceeded immediately with a pseudo-linear decrease of cell potential, suggesting no cell conditioning took place. The linear decrease of cell potential continued for approx. 10 minutes, after which time non-linear behaviour was observed, and the cell potential fell more rapidly for approx. 5 minutes until reaching approx. 0.46 V. After this first phase of discharge, the cell potential decreased more erratically, eventually reaching the cut-off voltage after 35-40 minutes.

A mass balance profile was measured to show how the mass of the steel anode changed during discharge. This was measured by stopping the discharge process every minute, and then removing, drying (air drying at room temperature) and weighing the steel electrode, before replacing it back into the cell and restarting the discharge. This was repeated until no mass loss was measured in order to

build up a picture of mass loss from the steel throughout the discharging process. The mass loss profile is shown in Fig. 5, with approx. 0.004-0.008 g of material lost during every minute of discharge (incremental mass removal). The cumulative mass loss indicated that removal of mass proceeded in a pseudo-linear manner for 21 minutes, after which time no more material was removed. The majority of mass loss coincided with the first phase of discharge observed in Fig. 4, which was complete within approx. 15 minutes. Some loss of mass from the steel anode continued during the second phase but was not observed for the whole duration of this second phase.

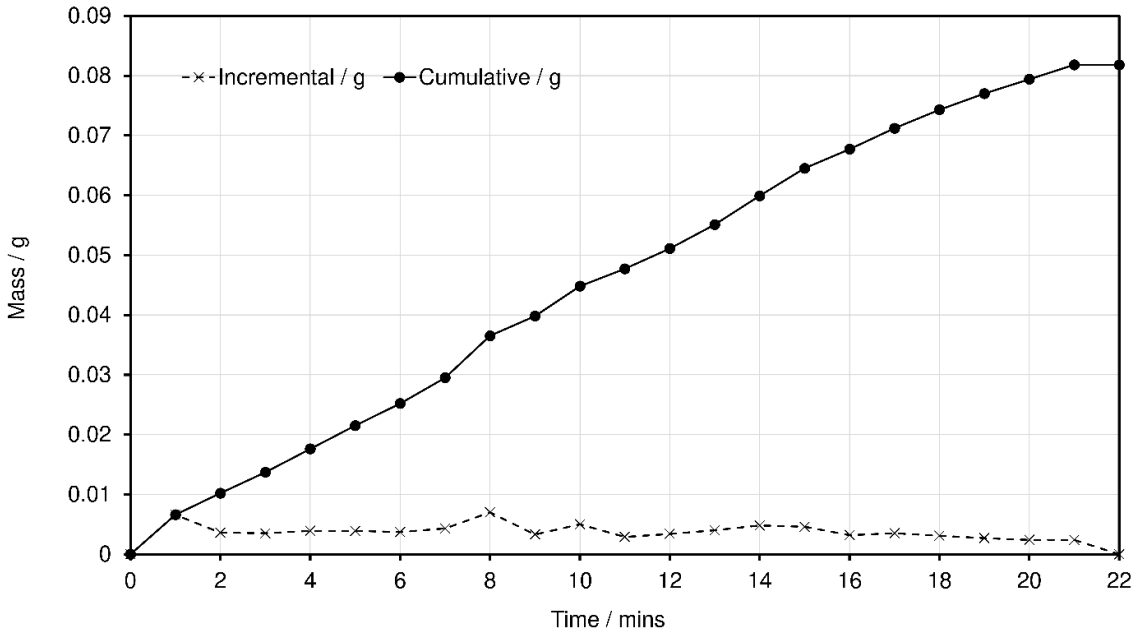

Figure 5. Incremental and cumulative removal of mass from steel during cell discharge.

Following discharge, each steel anode studied in this work was removed from the cell and allowed to air dry at room temperature, with a representative photograph shown in Fig. 6a. Each steel electrode was not dipped fully into the electrolyte solution in order to allow comparison of the steel before and after discharge. The area of steel not dipped into the electrolyte solution had a lighter silver-grey appearance, whereas the steel that was dipped into the electrolyte exhibited two types of corrosion. The development of a dark brown/orange rust formed most of the observed corrosion, but there were also areas with a grey appearance darker than the original silver/grey appearance of galvanised steel. Both forms of corrosion did not take place uniformly over the surface of the steel and sometimes took several

days after discharge and drying to develop. This is attributed to imperfect surface coating of zinc during the galvanisation process, with minute differences in zinc layer thicknesses present across steel surfaces.

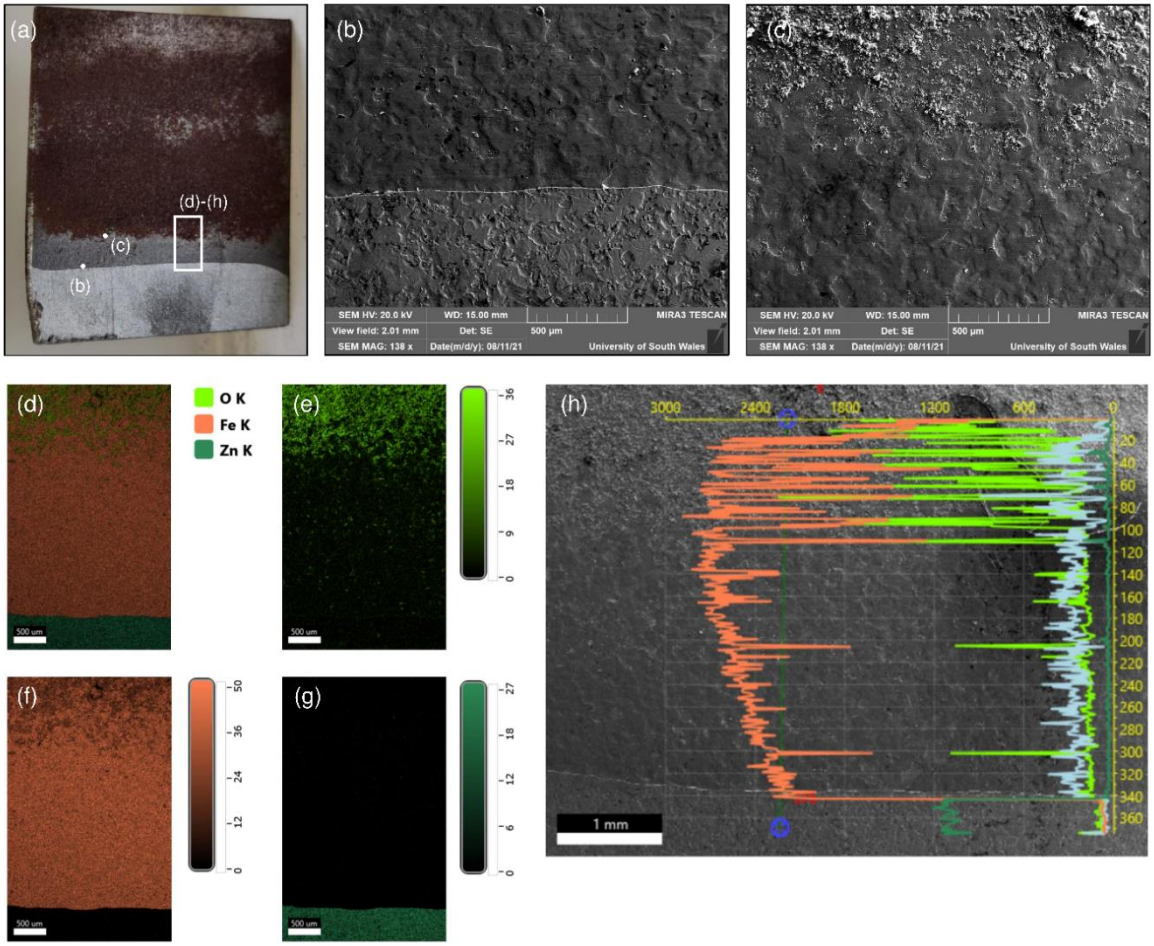

Figure 6. (a) Representative photograph of steel anode after cell discharge, removal from the cell and drying. (b) and (c) are SEM secondary electron images taken at the positions indicated in part (a). (d-g) show SEM-EDS elemental mapping spectra of the steel after discharge for all elements (d) and then separately for oxygen, iron and zinc in (e), (f) and (g) respectively. (h) shows an SEM-EDS elemental line spectrum of the steel.

SEM secondary electron images of the steel were measured following discharge and are shown in Figs. 6b and 6c. Fig. 6b compares the dark-grey corrosion with the initial steel surface and revealed this corrosion yielded a smoother surface. Fig. 6c shows rusting also gave a smooth surface but with powder-like deposits scattered across the top. The presence of elements on the surface of the steel anode was

analysed using SEM-EDS, with mapping spectra shown in Figs. 6d-g and a line spectrum shown in Fig. 6h. Fig. 6g shows the initial steel surface was composed entirely of zinc, with zinc clearly present on the steel not exposed to the electrolyte solution (at the bottom of the image), and with no zinc detected anywhere else. This demonstrates the cell was very effective in removing zinc from steel surfaces, with more than 99.9 % removal achieved and with less zinc remaining on the surface than the lower detection limit of the EDS detector. Figs. 6d-f show that following removal of zinc, the steel surface was composed mostly of iron with lower levels of oxygen present, suggesting the surface was composed of a mixture of metallic iron and iron oxide. The is corroborated by line spectrum in Fig. 6h, which shows that after removal of zinc, the presence of iron and oxygen increased as the distance from the electrolyte surface increased.

The discharge profile measured with a standard carbon foam anode agreed with observations from previous work[36, 45] and reflects the depletion of metallic zinc and bromine liquid reactants. However, the results and observations in Figs. 3-6 strongly suggest that a two-stage discharge process took place with the steel anode and that this was due to the removal of zinc in the first stage, followed by removal of iron in the second stage. Fig. 5 shows that almost all of the mass removal from the steel took place within the first stage of discharge, with most of this mass likely to be zinc, since zinc was the only element initially exposed on the steel surface (as confirmed by the SEM-EDS measurements) and would have faster desorption kinetics in this type of cell than metallic iron. Following zinc removal, metallic iron was exposed to the electrolyte solution and it is proposed that the cell then extracted iron into the aqueous phase, resulting in a second phase of discharge. This agrees with the physical observations of the battery appearance shown in Fig. 3, where the electrolyte had a dark brown and opaque appearance, resembling aqueous iron, rather than the transparent deep orange and yellow colours characteristic of bromine liquid and its complexes. In addition, at the start of the second discharge phase, the cell potential was approx. 0.46 V, which is close to the magnitude of the standard electrode potential of Fe^{2+} of 0.44 V. The slow decline of cell potential during the second phase of discharge reflects the slow kinetics of iron desorption into the electrolyte. Fig. 4 shows discharge with steel took place for longer than 35 minutes, suggesting therefore that the removal of mass (iron) also continued for this length of

time. However, mass removal was not measured after 21 minutes of discharge (see Fig. 5) and it is suggested that mass removal could not be measured for the whole duration of this phase since the incremental mass removed within a minute of operation was too low. Further work is required to determine the mechanism of iron extraction and the interaction of aqueous iron ions with the electrodes and metallic zinc present within the cell.

Multi-cycle characterisation

Multi-cycle measurements were conducted in order to gain insight into the durability of the cell as well as the capability of the cell to recover zinc. Fig. 7 shows the profiles of 25 charge-discharge cycles for the cell measured using a carbon foam anode under charging and then discharging with galvanised steel anodes with a cut-off voltage of 0.2 V. The average coulombic efficiency was 61 % with a relative standard deviation 21.9%. The charging voltage was variable and averaged between 1.7-2.0 V, sometimes maintaining a stable value throughout charging, although in the majority of cycles the charging voltage was transient and sometimes erratic. In some cases, the voltage initially jumped to a very high value (> 3.0 V), or a slightly lower value (~ 1.5 V) before rapidly going to 1.7-2.0 V. In many cycles, the voltage decreased slowly during charging, and in a few cycles the voltage remained constant. After cycle 25, it was not possible to start another charging cycle because the voltage rapidly increased above the limit of the potentiostat (> 9 V), indicating the cell had undergone irreversible degradation.

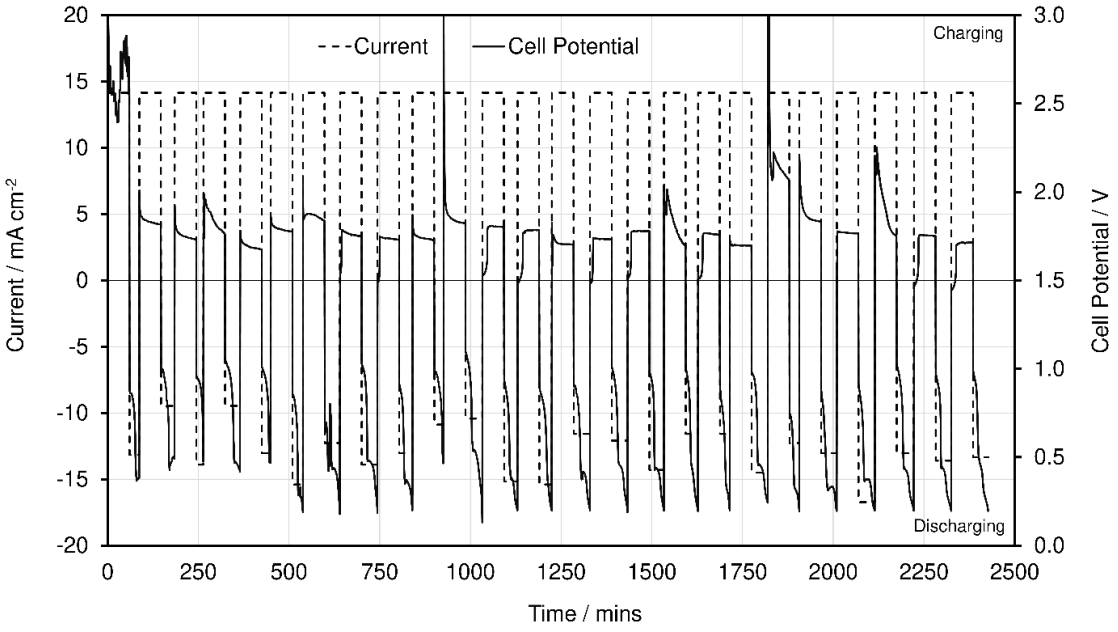

Figure 7. Charge-discharge profile of the ZBB cell over 25 cycles. The cell was charged at 100 mA (14.15 mA cm^{-2}) using a carbon foam anode. The carbon anode was then replaced with galvanised steel for discharge at 100 mA. A cut-off voltage of 0.2 V was used when discharging.

After measuring these charge-discharge profiles, the carbon foam anode and cathode were removed from the cell and air dried at room temperature. SEM secondary electron images of the electrodes were measured with a corresponding EDS elemental map (see Fig. 8). In Figs. 8a and 8b, the carbon foam fibres were observed as strands of dark material across the image and were embedded within a porous and roughly textured material. The elemental analysis confirmed the solid material was mainly composed of zinc, although crucially there was a clear presence of iron (~ 5 wt%), confirming that under discharge, the cell removed iron from the steel anodes as well as zinc and that this iron ultimately became adsorbed onto the surface of carbon foam electrodes. It is likely the iron was a major cause of the irreversible cell degradation observed after cycle 25. Some bromine was detected, which was expected since the work was conducted with a membrane-free (static) design where the bromine was able to flow freely between the electrodes. However, SEM-EDS is a surface analysis technique and the amount of bromine present within the bulk of the electrode and crystals was likely to be very low. Oxygen was present, although the form it was present in is not clear from these measurements alone.

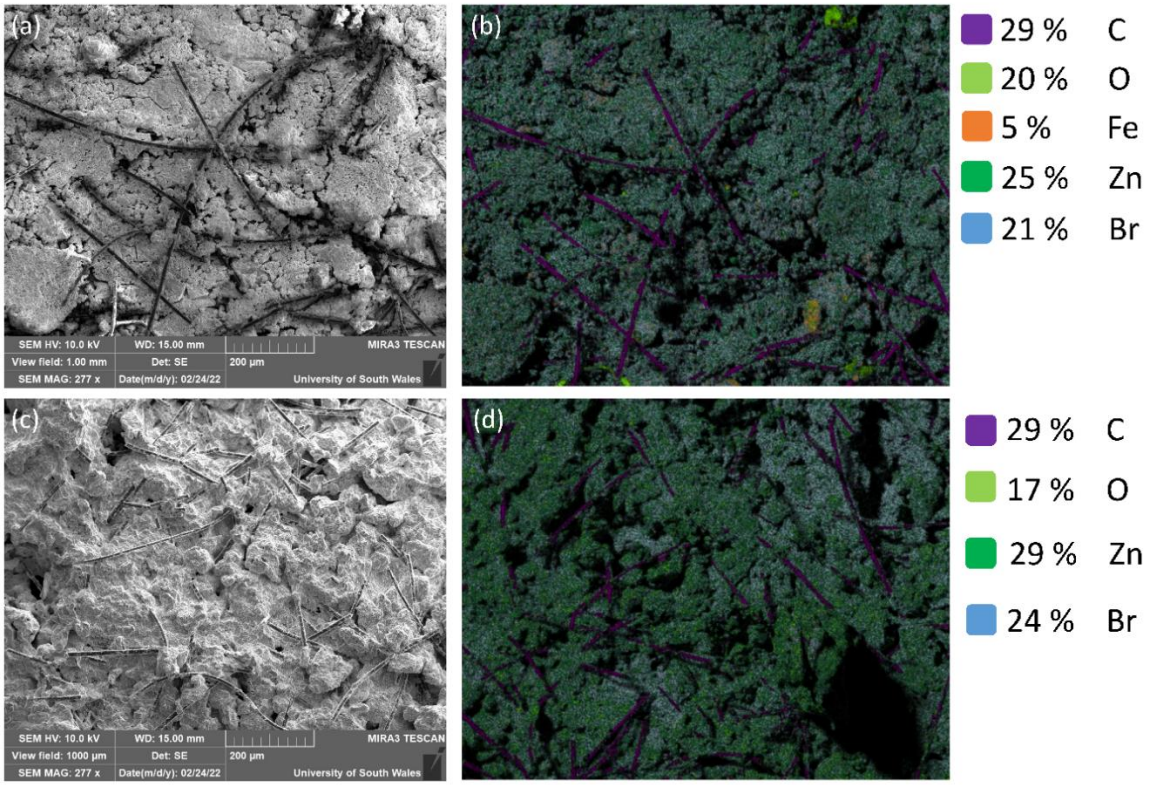

Figure 8. (a) SEM secondary electron image and (b) elemental map of the carbon foam anode after 25 cycles of charge-discharge using a 0.2 V cut-off voltage. (c) SEM secondary electron image and (d) elemental map of the carbon foam anode after 30 cycles of charge-discharge using a 0.5 V cut-off voltage.

Figs. 9a and 9b show SEM images and data of the carbon foam cathode of the cell after 25 cycles with a 0.2 V cut-off voltage. Fig. 9a shows the carbon fibres were lightly coated with residue, rather than being embedded within a solid structure. In many instances, the fibres had become clumped together by the residue within the electrode. The EDS mapping analysis shows the residue mainly consisted of bromine, although again there was a clear presence of iron observed, confirming that iron extracted from the steel was distributed completely through the electrolyte solution, with some deposited onto the cathode as well as the anode. Zinc was also deposited within the bromine electrode and formed ~ 12 wt% of the surface elemental composition. Like the anode, a small amount of oxygen was present, but the precise form could not be determined.

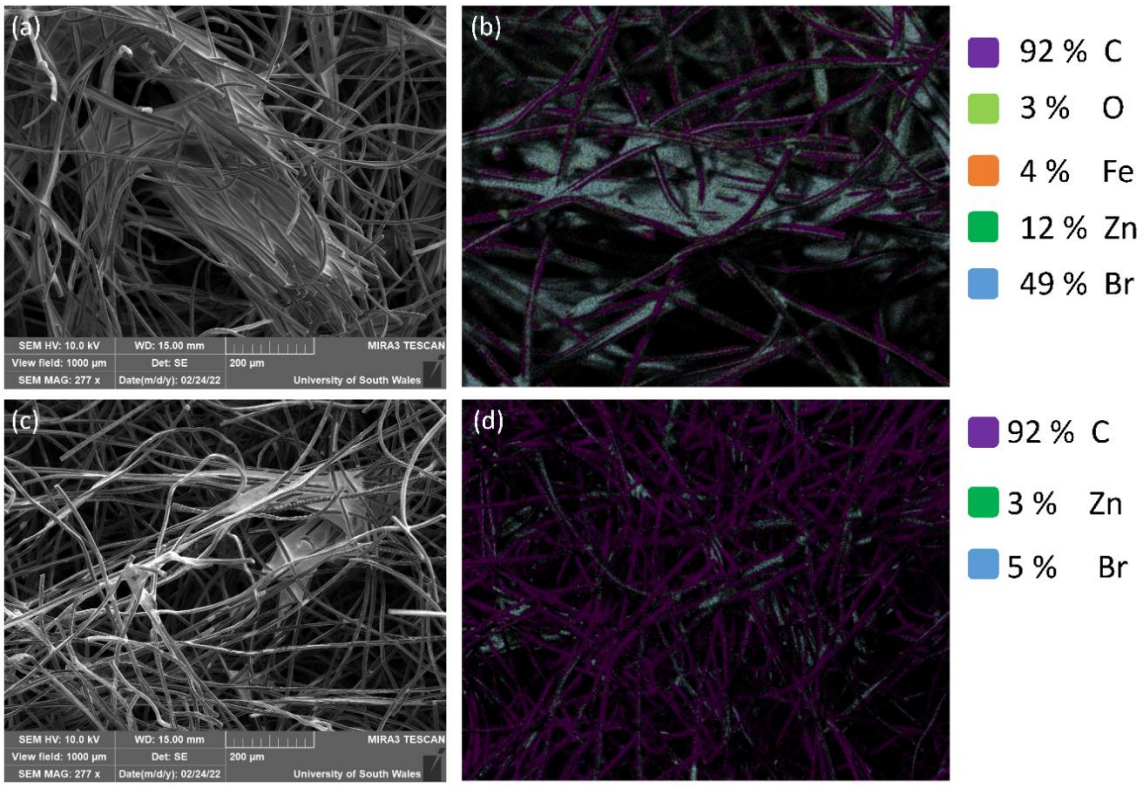

Figure 9. (a) SEM secondary electron image and (b) elemental map of the cathode after 25 cycles of charge-discharge using a 0.2 V cut-off voltage. (c) SEM secondary electron image and (d) elemental map of the cathode after 30 cycles of charge-discharge using a 0.5 V cut-off voltage.

These charge-discharge profile measurements confirmed that the extraction of iron posed a significant problem to the durability and long-term operation of the cell for extracting zinc from steel. For many of the cycles, the second stage of discharging did not take place until the voltage of the cell had dropped below 0.5 V. Therefore, in order to limit iron extraction and improve the durability of the cell, the charge-discharge profile measurements were repeated using a 0.5 V cut-off voltage. Fig. 10 shows no discharge cycles took place in two-stages. The cell discharged rapidly, with a much lower average coulombic efficiency of 32.0 % and relative standard deviation of 31.5 % measured. The behaviour of the cell under charging was less erratic than with a 0.2 V cut-off voltage, and higher average charging voltages of between 1.9-2.3 V were measured. In general, there was less variation and less erratic transient behaviour observed when using a 0.5 V cut-off voltage. The average charging voltage appeared to increase steadily during the last 10 cycles and this is tentatively attributed to over-charging

of the cell and decreasing reactant concentration in the electrolyte solution. A total of 30 cycles were measured, which was more than the 0.2 V cut-off profiles, and no significant deactivation of the cell was observed; it is the expectation that the cell could have operated for many more cycles. However, it was decided to disassemble the cell in order to analyse the components of the cell after a comparable number of cycles to that measured for the 0.2 V cut-off voltage measurements.

When analysing the electrodes under SEM/EDS, many of the observations described for the 0.2 V cut-off voltage electrodes were made using 0.5 V electrodes. The main difference was the level of iron detected, which was absent from both 0.5 V electrodes. The improved long-term performance and absence of iron confirm that the two-stage discharge process and the long-term operation problems were both ultimately attributed to the low 0.2 V cut-off voltage and subsequent extraction of iron. These were straightforwardly avoided by selecting a cut-off voltage higher than the voltage where the second phase of discharge (and therefore iron extraction) started.

In addition, the increased cut-off voltage improved the condition of the carbon foam electrodes. The purity of zinc at the anode was higher and the SEM secondary electron image in Fig. 8c shows the material was less porous and more crystalline in appearance. There was some bromine detected again, but this was only likely to be residual levels on the surface and not within the bulk of the material, thereby forming a negligible fraction of the material as a whole. There was also less accumulation of material in the cathode, with carbon forming the majority of the material and with less zinc, bromine and oxygen measured. This suggests the performance of the anode was improved due to the reactants and products moving into and out of the foam at a faster rate. The iron present in the 0.2 V cut-off voltage electrodes was likely to have hindered the diffusion of materials through the electrode, and therefore promoted their accumulation and ultimately made the performance of the cell more erratic between cycles.

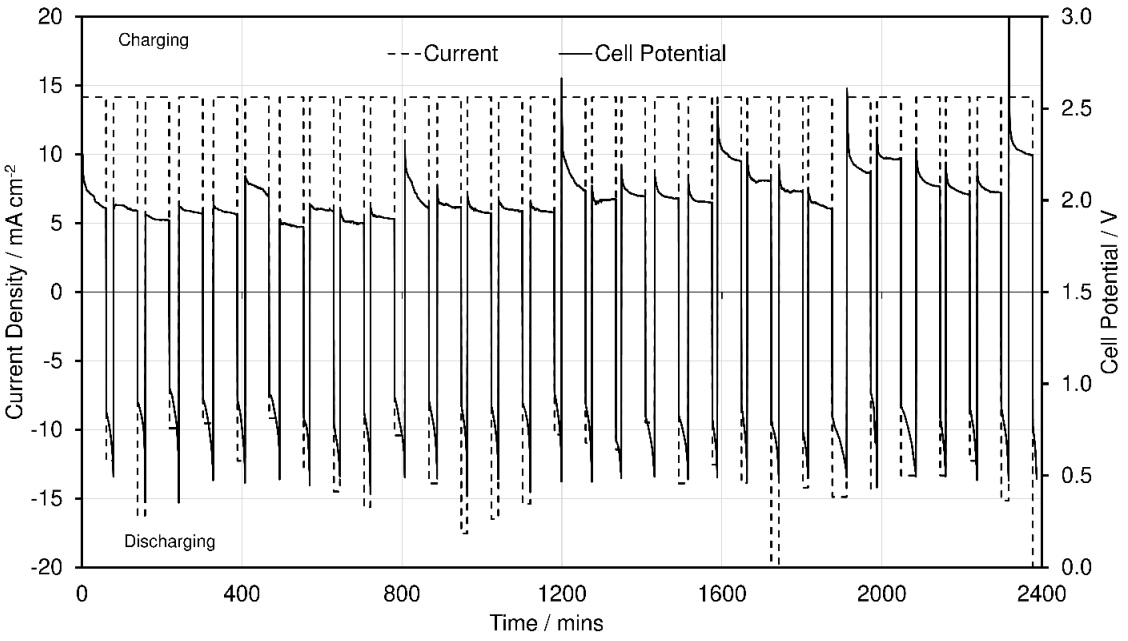

Figure 10. Charge-discharge profile of a zinc bromine battery over 30 cycles. The cell was charged at 14.15 mA cm^{-2} using a carbon foam anode. The carbon anode was then replaced with galvanised steel for discharge at 100 mA. A cut-off voltage of 0.5 V was used when discharging.

Figure 11 shows how the discharge time and zinc removed varied over the charge-discharge profile cycles when using 0.2 V and 0.5 V cut-off voltages, with further data provided in Table 1. For both cut-off voltages, there was a strong correlation between discharge time and mass of material removed: if there was more zinc present, the discharge time was longer, and the mass of material removed was higher. For the 0.2 V cut-off cycles, the average discharge time (36.58 minutes) and mass removal (104.8 g m^{-2}) was higher due to the second phase of discharge, which increased the time taken for the battery to reach 0.2 V and therefore the apparent coulombic efficiency increased. The mass of material removed was also higher, although a greater fraction was composed of iron. When using a 0.5 V cut-off voltage, the average discharge time (19.68 minutes) and mass removal (62.48 g m^{-2}) were lower since the second phase of discharge was avoided, decreasing the apparent coulombic efficiency. However, the SEM measurements show zinc was removed selectively from the steel without iron extraction. The higher purity of zinc obtained accounts for the lower quantity of material removed with the 0.5 V cut-off voltage (1.39 g) compared with the materials collected with a 0.2 V cut-off voltage

(2.04 g). The zinc recovery rate was 31.36 % with the 0.5 V cut off voltage and 40.86 % with the 0.2 V cut off voltage. Whilst these are lower than the recovery yields of approx. 90 % that can be achieved with pyrometallurgical processes, there is scope to optimise cells for zinc recovery and there were no harmful substances produced by the ZBB system, which offers much cleaner zinc recovery. Further work is required to investigate the mass balances for zinc recovery using ZBBs, before optimising and scaling up the process for deployment with real scrap steel and zinc-containing waste streams.

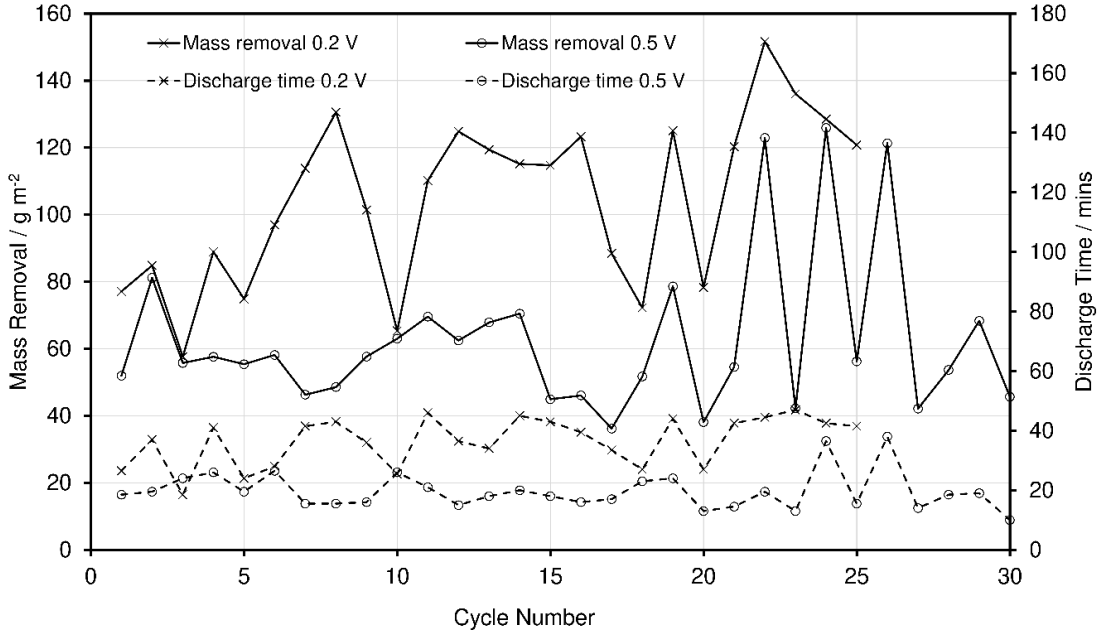

Figure 11. The mass removed and discharge time for each of the charge-discharge profile cycles measured using 0.5 V and 0.2 V cut-off voltages.

Regardless of the cut-off voltage used, there was clear variation in discharge time and mass removed between cycles. This is attributed to variation in thickness of the zinc coating of the surface in between pieces of steel. The manufacturer specification was 100 g of zinc per square metre (total for both sides), which is 0.005 g cm^{-2} per side. Due to imperfections in the manufacturing process, variation in the actual quantity of zinc present is to be expected and accounts for the variation in performance observed between cycles. The standard deviation of discharge time and mass removal were slightly lower for the 0.5 V cut-off cycles, showing the higher cut-off voltage alleviated variation to a degree.

Table 1. Mass balance and efficiency data for recovery of zinc from steel using a zinc-bromine battery cell.

	Cut-off voltage: 0.2 V	Cut-off voltage: 0.5 V
Total mass of material removed / g	2.0376	1.3907
Total mass of material recovered / g	0.8325	0.4361
Percentage yield	40.86 %	31.36 %
Average discharge time / mins	36.58	19.68
Discharge time standard deviation / mins	8.00	6.20
Discharge time relative standard deviation	21.86 %	31.52 %
Average mass removal / g m^{-2}	104.8	62.48
Mass removal standard deviation / g m^{-2}	24.32	23.04
Mass removal relative standard deviation	23.20 %	36.87 %

Implications for zinc recovery from scrap steel

The results presented in this work show zinc-bromine battery technology could potentially be used to remove and recover zinc present in waste or scrap steel. This is firstly made possible by the static, membrane-free design, where the battery has an open top, leaving the electrolyte solution exposed and enabling electrodes and scrap or steel substrates to be easily dipped into and removed from the battery system. In theory, the zinc substrate could be any size or shape, provided it is within the dimensions of the cell housing. Zinc-bromine batteries are scalable devices and could be made to any size appropriate to the steel substrates as required. Provided the substrate is electronically conductive, they could be dipped into the top of the battery system and discharged to remove the zinc from the surface of the substrate and into the electrolyte solution (see Fig. 12). The battery would require charging prior to this stage in order to generate the liquid bromine in the cell required for the battery to produce zinc bromide upon discharging. Discharging would also yield electrical power, which could be used for on-site

industrial processes, exported to the electricity grid or stored and used for the battery charging for example. Once discharge is complete, the steel substrate would then be removed and re-used or recycled as required.

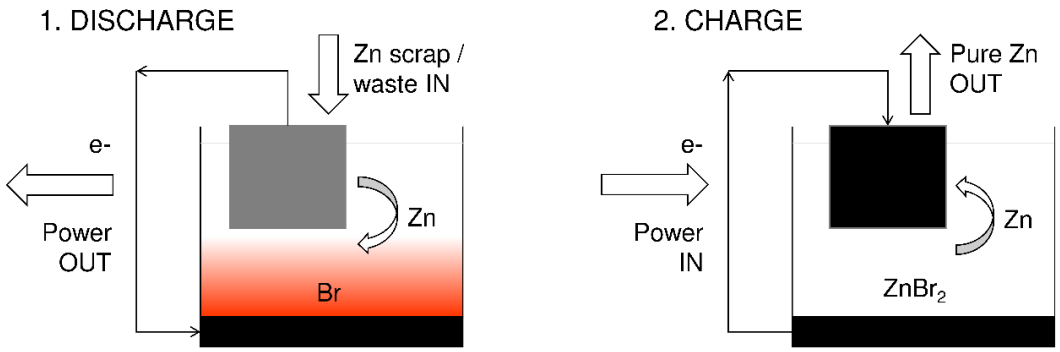

Figure 12. Schematic depicting the principle of using ZBB technology to remove and recover pure zinc from scrap steel.

In order to recover the zinc removed from the steel, the battery would then be recharged by inserting a conventional carbon foam electrode into the electrolyte solution and applying electrical load to the cell. This power could be sourced from the electricity grid or renewable source. Under charging, the zinc bromide would be electrolysed to regenerate the liquid bromine and electroplate the zinc metal onto the carbon electrode. Once charging is complete, the carbon electrode can be removed, leaving the battery system ready to discharge the next steel substrate. The carbon electrode could be re-used in subsequent charging cycles in order to accumulate zinc. It would then be replaced once saturated.

The results presented in this work suggest the ZBB cell is robust and able to operate over many cycles. In addition, the yield and purity of zinc generated on the carbon electrode is high, and no harmful by-products or secondary waste streams are produced. The system operates at relatively low concentrations of bromine and as such, no bromine vapours are released from the battery despite the electrolyte solution being exposed to the atmosphere. Further work is required to investigate process scale-up and fully determine the mass balance and energy efficiency of the process.

Conclusion

In order for the steel industry to achieve net zero targets, technical innovations will be required to enable green steel manufacturing as well as effective and efficient processes for recycling and re-using scrap, waste and by-product streams. At present, only 40 % of steel is produced via secondary methods (recycling), which is proven to decrease CO_2 emissions compared with primary steelmaking from iron ore. The difficulties of recycling steel relate to end-of-life scrap which, due to imperfect separation processes, typically contains a range of alloys and is usually contaminated with non-ferrous metals and non-metal debris. These contaminants include zinc which is usually present on steel surfaces as a protective barrier towards corrosion. Blast furnace and electric arc systems have a low tolerance (< 0.02 wt%) towards zinc, making direct remelt recycling difficult.

In this work, the recovery of zinc from the surface of steel substrates was investigated using a custom-made membrane-free non-flow zinc-bromine battery (ZBB). The battery was designed in order to allow fast and easy integration and removal of steel substrates and was made with low-cost materials. The electrical performance of the cell was characterised by charge-discharge profiles and zinc removal and recovery onto electrodes was characterised using Scanning Electron Microscopy (SEM) and Energy Dispersive Spectroscopy (EDS). Upon discharging, the cell efficiently and quickly removed > 99.9 wt% zinc from steel surfaces. On recharging the cell, zinc was re-electroplated onto a carbon foam electrode in an easily recoverable form and with high purity. Operation of the cell for this purpose was demonstrated over 30+ cycles suggesting the cell was robust and durable. The work shows the importance of the cut-off voltage upon discharging: if less than 0.5 V, the cell co-extracted iron into the electrolyte solution, affecting cell durability and the purity of zinc recovered.

This work successfully demonstrates that ZBB technology could enable efficient and clean recovery of zinc from scrap steel and therefore help to increase steel recycling and secondary steel production rates and make the prospects for green steel production more realistic. With further work and modifications, the process developed could be used to treat slurries generated from basic oxygen steelmaking processes, and secondary vent dust from the primary steelmaking off gas streams. A two-stage process

for recovering zinc from scrap steel has been proposed. Future work should focus on establishing the mechanisms and mass balance of ZBB operation for zinc recovery, improving the durability of the cell, improving zinc recovery yields as well as exploration into other steel waste products such as dusts and sludges from blast furnaces.

Experimental Section

Preparation of zinc–bromine battery cell

A schematic of the cell studied in this work with photographs of individual components are shown in Fig. 13. The housing of the cell and the end-plates were composed of transparent perspex and the assembly was held together using nylon threaded bars (Falcon workshop supplies, B076492CLJ) fed through bore holes positioned in the four corners of the housing. The assembly was tightened using stainless steel butterfly wing nuts and tested for liquid tightness using deionised water. In between the bottom end-plate and the housing was a nitrile rubber gasket (RS Components, 681-586), a PV-15 bipolar plate (SGL) and 6 mm hydrophobic porous carbon felt cathode for bromine storage (SGL). For the electrolyte solution, an aqueous solution of 2 M zinc bromide (MERCK, 99 %, CAS 18921-13-6) was prepared and 25 mL was transferred into the electrolyte chamber of the cell using a 5 mL pipette (Thermo scientific Finnpipette F2 pipette, CAT: 4642010). At the top of the cell, there was an open-ended carbon plastic end-plate, enabling a 4.65 mm hydrophilic carbon anode for zinc plating (SGL) to be dipped into solution. This was attached to a crocodile clip held in position using a clamp stand. Connections to a potentiostat were made using crocodile clips attached to the bipolar plate (in the case of the bromine electrode) and directly onto either the carbon foam or steel anode (in the case of the zinc electrode).

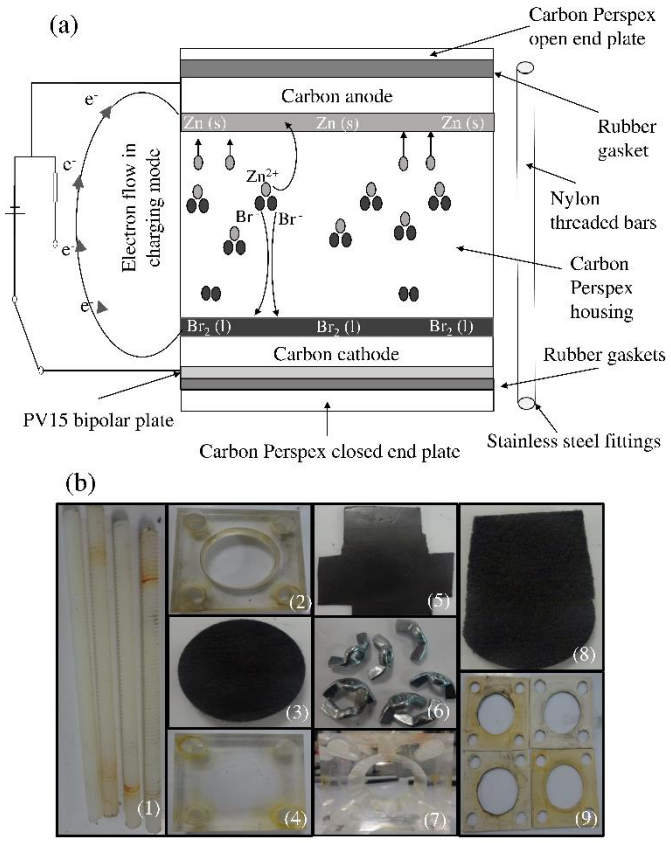

Figure 13. Construction and assembly of ZBB cell used in this work. (a) shows a schematic of the cell, (b) shows photographs of individual components (1) nylon threaded bars, (2) open ended carbon plastic end plate hydrophilic, (3) hydrophobic carbon cathode, (4) closed carbon plastic end plate, (5) PV15 bipolar plate, (6) stainless steel butterfly wing nuts, (7) carbon plastic cell housing, (8) suspended carbon electrode, (9) rubber seals.

Cell testing and characterisation

Charge-discharge cycles were measured using an Ivium Technologies Iviumstat.h potentiostat in a 2-electrode configuration with 4-wires. Each cycle consisted of charging the cell for 1 hour at a current density of 14.15 mA cm^{-2}, and subsequently discharging until a cut-off voltage of 0.2 V or 0.5 V was achieved (depending on the experiment). When discharging using a carbon foam zinc electrode, a current density of 14.15 mA cm^{-2} was used. When discharging using a steel substrate zinc electrode, a current of 100 mA was used. Due to the different sizes of steel substrate used, this corresponded to

current densities in the range 9-26 mA cm^{-2}. When discharging with steel substrates, the carbon anode was replaced with steel after charging and before discharge was started. All charging and discharging cycles were carried out using the Iviumsoft transients mixed mode tool.

Scanning electron microscopy (Tescan Tima 3 / Mira 3 x64) was used to characterize the microstructure of the electrodes. Samples were analysed with preparation or sample coating before introduction to the SEM. Images were taken using the secondary electron detected with a beam voltage in the range 10.0-20.0 kV. Elemental analysis was performed using energy dispersive spectroscopy (EDS).

Acknowledgements

The authors would like to acknowledge the funding provided for this work through the KESSII scheme (MAXI 21489). Knowledge Economy Skills Scholarships (KESS) is a pan-Wales higher-level skills initiative led by Bangor University on behalf of the HE sector in Wales. It is part funded by the Welsh Government's European Social Fund (ESF) programme for West Wales.

References

[1] K. H. Lo, C. H. Shek, J. K. L. Lai, *Mater. Sci. Eng. R Rep*. **2009**, *65*, 39–104.

[2] Iron and Steel Technology Roadmap: Towards More Sustainable Steelmaking, *Energy Technology Perspectives*, International Energy Agency, IEA Publications, Paris, **2020**. https://www.iea.org/reports/iron-and-steel-technology-roadmap [accessed 12 April 2022].

[3] L. D. D Harvey, *Renew. Sust. Energ. Rev.* **2021**, *138*, 110553.

[4] C. Broadbent, *Int. J. Life. Cycle. Assess*. **2016,** *21*, 1658–1665.

[5] N. C. C. Lobato, E. A. Villegas, M. B. Mansur, *Resour. Conserv. Recycl.* **2015**, *102*, 49–57.

[6] A. R. Mander, *Prog. Mater. Sci.* **2000,** *45*, 191–271.

[7] D. J. C Stewart, A.R. Barron, *Resour. Conserv. Recycl.* **2020**. *157*, 104746.

[8] D. J. C. Stewart, A. Scrimshire, D. Thomson, P. A. Bingham, A. R. Barron, *Resour. Conserv. Recycl.* **2022**, *14*, 200073.

[9] P. Besta, K. Janovská, A. Samolejová, A. Beránková, I. Vozňáková, M. Hendrych, *Metalurgija,* **2013**, *52*, 197–200.

[10] B. Björkman, C. Samuelsson. *Recycling of steel.* (Eds: E. Worrell, M.A Reuter), Elsevier, Amsterdam, **2014**, 65–83.

[11] I. Daigo, S. Osako, Y. Adachi, Y. Matsuno, *Resour. Conserv. Recycl.* **2014**, *82*, 35–40.

[12] J. Wang, Y. Zhang, K. Cui, T. Fu, J. Gao, S. Hussain, T. S. AlGarni, *J. Clean. Prod.* **2021**, *298*, 126788.

[13] B. Lin, X.Wang, *Renew. Sust. Energ. Rev.* **2015**, *47*, 746–754.

[14] K. Mager, U. Meurer, B. Garcia-Egocheaga, N. Goicoechea, J. Rutten, W. Saage, F. Simonetti, *Recovery of Zinc Oxide from Secondary Raw Materials: New Developments in the Waelz Process*. (Eds. D.L. Stewart, J.C. Daley, R.L. Stephens), Recycling of Metals and Engineered Materials, **2013**.

[15] L. M. Simonyan, A. A. Alpatova, N. V. Demidova, *J. Mater. Res. Technol.* **2019**, *8*, 1601–1607.

[16] H. Bindra, S. T. Revankar, *Storage and Hybridization of Nuclear Energy. Techno-economic Integration of Renewable and Nuclear Energy*. Academic Press. (Eds. H. Bindra, S.T. Revankar), **2018**, ch 6. pp 177–227.

[17] Q. Lai, H. Zhang, X. Li, L. Zhang, Y. Cheng, *J. Power. Sources*. **2013**, *235*, 1–4.

[18] W.A. Braff, C. R. Buíe, M. Z. Bazant, *J. Electrochem. Soc*. **2013**, *160*, A2056.

[19] L. Amit, D. Naar, R. Gloukhovski, G. J. la O', M. E. Suss, *ChemSusChem* **2021**, *14*, 1068–1073.

[20] L. Zhang, Q. Lai, J. Zhang, H. Zhang, *ChemSusChem*. **2012**, *5*, 867–869.

[21] J. D. Milshtein, S.L. Fisher, T. M. Breault, L. T. Thompson, F. R. Brushett, *ChemSusChem*. **2017**, *10*, 2080–2088.

[22] S. Suresh, T. Kesavan, Y. Munaiah, I. Arulraj, S. Dheenadayalan, P. Ragupathy, *RSC Adv*. **2014**, *4*, 37947

[23] B. Dunn, H. Kamath, J. M. Tarascon, *Science* **2011**, *334*, 928–935.

[24] H. Zhang, W. Lu, X. Li, *Electrochemistry* **2019**, *2*, 492–506.

[25] M. Darling, K. G. Gallagher, J. A. Kowalski, S. Ha, F. R. Brushett, *Energy Environ*. Sci. **2014**, *7*, 3459–3477.

[26] Z. Xu, Q. Fan, Y. Li, J. Wang, P. D. Lund, *Renew*. *Sust*. *Energ*. *Rev*. **2020**, *127*, 109838.

[27] H. R. Jiang, M. C. Wu, X. Y. Ren, W. Shyy, T. S. Zhao, *Appl*. *Energy*. **2018**, *213*, 366–374.

[28] Y. Shao, M. Engelhard, Y. Lin, *Electrochem. Commun.* **2009**, *11*, 2064–2067.

[29] R. A. Putt, Final Report Gould Inc Rolling Meadows IL; **1979**.

[30] G. P. Rajarathnam, A.M. Vassallo, *The Zinc/Bromine flow battery. Materials Challenges and Practical Solutions for Technology Advancement*. Springer Singapore, **2015**.

[31] P. K. Adanuvor, *J. Electrochem. Soc*. **1987**, *134*, 1450.

[32] G. P. Rajarathnam, A. Montoya, A. M. Vassalo, *Electrochim. Acta*. **2018**, *292*, 903–913.

[33] A. K. Neufeld, I. S. Cole, A. M. Bond, S. A. Furman, *Corros*. *Sci*. **2002**, *44*, 555–572.

[34] R. Kim, H. G. Kim, G. Doo, C. Choi, S. Kim, J-H. Lee, J. Heo, H-Y. Jung, H-T. Kim, *Sci. Rep*. **2017**, *7*, 10503.

[35] M. Schneider, G. P. Rajarathnam, M. E. Easton, A. F. Masters, T. Maschmeyer, A. M. Vassallo, *RSC Adv*. **2016**, *6*, 110548–110556.

[36] R. Kim, S. Yuk, J-H. Lee, C. Choi, S. Kim, J. Heo, H-T. Kim, *J. Membr. Sci.* **2018**, *564*, 852–858.

[37] D. Han, S. Shanmugam, *J. Power. Sources.* **2022**, *540*, 231637.

[38] D. M. Rose, S. R. Ferreira, United States: N. **2013**, Web.

[39] M. Kim, A. Yun, J. Jeon, *J. Power. Sources.* **2019**, *438*, 227020.

[40] M. Wu, T. Zhao, R. Zhang, H. Jiang, L. Wei, *Energy. Technol.* **2018**, *6*, 333–339.

[41] J. Jeon, H. Sun, J. Shim, H. Sik, J. Hoon, *Electrochim. Acta* **2014**, *127*, 397–402.

[42] J. H. Yang, H. S. Yang, H. W. Ra, J. Shim, J. D. Jeon, *J. Power. Sources* **2015**, *275*, 294–297.

[43] E. Lancry, B. Z. Magnes, I. Ben-David, M. Freiberg, *ECS Transactions*. **2013**, *53*, 107–115.

[44] K. W. Knehr, R. Buline, T. Baldwin, E. Guzman, H. Huynh, R. E. Ciez, D. A Steingart, *J. Electrochem. Soc.* **2018**, *165*, A4041.

[45] L. Gao, Z. Li, Y. Zou, S. Yin, P. Peng, Y. Shao, X. Liang, *iScience*. **2020**, *23*, 101348.

[46] S. Biswas, A. Semju, R. Mohr, T. Hodson, N. Karthikeyan, K. Knehr, A. G. Hsieh, X. Yang, B. E. Koel, D. A. Steingart, *Energy Environ. Sci.* **2017**, *10*, 114–120.